

- Invest.* **81**, 531 (1988).
16. B. Schleiffenbaum, R. Moser, M. Patarroyo, J. Fehr, *J. Immunol.* **142**, 3537 (1989).
  17. M. G. Tonnesen *et al.*, *J. Clin. Invest.* **83**, 637 (1989).
  18. D. C. Anderson, L. J. Miller, F. C. Schmalstieg, R. Rothlein, T. A. Springer, *J. Immunol.* **137**, 15 (1986).
  19. S. D. Marlin and T. A. Springer, *Cell* **51**, 813 (1987).
  20. M. W. Makgoba *et al.*, *Nature* **331**, 86 (1988).
  21. C. W. Smith, S. D. Marlin, R. Rothlein, C. Toman, D. C. Anderson, *J. Clin. Invest.* **83**, 2008 (1989).
  22. J. P. Buyon *et al.*, *J. Immunol.* **140**, 3156 (1988).
  23. M. R. Philips, J. P. Buyon, R. Winchester, G. Weissman, S. B. Abramson, *J. Clin. Invest.* **82**, 495 (1988).
  24. N. B. Vedder and J. M. Harlan, *ibid.* **81**, 676 (1988).
  25. S. K. Lo, P. A. Detmers, S. M. Levin, S. D. Wright, *J. Exp. Med.* **169**, 1779 (1989).
  26. W. Smith, J. R. Gamble, M. A. Vadas, in preparation.
  27. S. K. Lo, G. A. Van Seventer, S. M. Levin, S. D. Wright, *J. Immunol.* **143**, 3325 (1989).
  28. M. P. Bevilacqua *et al.*, *J. Clin. Invest.* **76**, 2003 (1985).
  29. F. W. Luscinskas, A. F. Brock, M. A. Arnaout, M. A. Gimbrone, Jr., *J. Immunol.* **142**, 2257 (1989).
  30. R. Moser, B. Schleiffenbaum, P. Groscurth, J. Fehr, *J. Clin. Invest.* **83**, 444 (1989).
  31. G. A. Zimmerman, T. M. McIntyre, S. M. Prescott, *ibid.* **76**, 2235 (1985).
  32. J-G. Geng *et al.*, *Nature* **343**, 757 (1990).
  33. T. K. Kishimoto, M. A. Jutila, E. L. Berg, E. C. Butcher, *Science* **245**, 1238 (1989).
  34. J. R. Gamble, M. J. Elliott, E. Jaipargas, A. F. Lopez, M. A. Vadas, *Proc. Natl. Acad. Sci. U.S.A.* **86**, 7169 (1989).
  35. J. R. Gamble and M. A. Vadas, *J. Immunol. Methods* **109**, 175 (1988).
  36. Y. Saegusa, D. Cavender, M. Ziff, *J. Immunol.* **141**, 4140 (1988).
  37. R. T. Wall, L. A. Harker, L. J. Quadracci, G. E. Striker, *J. Cell. Physiol.* **96**, 203 (1978).
  38. We thank A. Lopez for helpful discussions; F. Bilogrevic and T. Browning for technical assistance; the staff of the delivery ward at The Queen Victoria Hospital, Adelaide, for collection of the umbilical cords; the staff at the Red Cross Blood Bank, Adelaide, for preparation of blood packs; Genentech, South San Francisco, for TNF- $\alpha$ ; P. Beatty, Fred Hutchinson Cancer Center, Seattle, for the gift of the monoclonal antibodies 60.1, 60.3, and 60.5; and M. Walker and B. Meakins for manuscript preparation. Supported by grants from the National Health and Medical Research Council (NH & MRC) of Australia and the National Heart Foundation. M.P.S. is the recipient of an NH & MRC postgraduate fellowship and M.C.B. of a Wellcome Senior Research Fellowship.

5 December 1989; accepted 8 May 1990

## Functional Organization of Primate Visual Cortex Revealed by High Resolution Optical Imaging

DANIEL Y. TS'O, RON D. FROSTIG, EDMUND E. LIEKE, AMIRAM GRINVALD

**A high spatial resolution optical imaging system was developed to visualize cerebral cortical activity in vivo. This method is based on activity-dependent intrinsic signals and does not use voltage-sensitive dyes. Images of the living monkey striate (V1) and extrastriate (V2) visual cortex, taken during visual stimulation, were analyzed to yield maps of the distribution of cells with various functional properties. The cytochrome oxidase-rich blobs of V1 and the stripes of V2 were imaged in the living brain. In V2, no ocular dominance organization was seen, while regions of poor orientation tuning colocalized to every other cytochrome oxidase stripe. The orientation tuning of other regions of V2 appeared organized as modules that are larger and more uniform than those in V1.**

**I**N THE MAMMALIAN NEOCORTEX, CELLS with similar functional properties are often grouped together into columns that run vertically from the pial surface to the white matter (1, 2). A striking demonstration of functional segregation can be seen in striate cortex (V1) when it is histochemically stained for cytochrome oxidase (3). A pattern of densely stained patches or blobs is revealed (4) among regions of lighter staining (interblobs). The blobs contain cells that are unoriented, monocular, and often color-selective, whereas cells in the interblobs are selective for orientation but usually not for color (5). A different pattern of cytochrome oxidase staining is observed in the second visual area (V2) of the primate: a series of bands or stripes. The stripes of denser staining are of two types, thick and thin, alternate in a regular fashion, and are

separated by intervening lighter, or pale stripes (6, 7). Electrophysiological studies (8, 9) have shown that the thin stripes contain unoriented color cells, whereas the thick stripes contain oriented, disparity-sensitive cells.

These previous studies relied on postmortem histology to identify these cortical subdivisions and thus could not directly investigate identified cortical regions with a microelectrode. Cortical activity can now be mapped with optical imaging (10–13) to obtain successive maps of responses to many different stimuli from the same cortical region in vivo, follow variations in responses over time, and quickly map a relatively large cortical region.

Most in vivo optical imaging studies have used optical signals provided by voltage-sensitive dyes (11). However, it is desirable to avoid the use of extrinsic probes when their ability to provide higher temporal resolution is not required since the dyes may introduce several complications, including pharmacological side effects, phototoxicity, and uncertainties in staining. Here we have

used a system with high spatial resolution for the optical imaging of intrinsic, activity-related optical signals (14, 15) in mammalian cortex. We have directly imaged, in vivo, the organization of several functional properties of cells, as well as the blobs of V1 and the stripes of V2 (16).

We began each experiment by acquiring an image of the cortical surface with a charge-coupled device (CCD) camera (17–20). This initial image served as a guide for the positioning of electrodes and a reference for cortical movement and drift over time (Fig. 1A).

To demonstrate our ability to visualize the functional architecture of visual cortex without the use of voltage-sensitive dyes, we imaged the ocular dominance (Fig. 1B) and orientation (Fig. 1C) columns of V1 (2, 21). In addition to single-unit recordings that confirmed our ocular dominance and orientation maps (22), we also saw a close correspondence between our maps and maps obtained from postmortem techniques, such as 2-deoxyglucose (2-DG) autoradiography, cytochrome oxidase histology, and anterograde tracing. Our maps of ocular dominance and orientation tuning in V1, based on intrinsic signals, are similar to the maps of Blasdel and Salama (12), who used voltage-sensitive dyes. We analyzed our orientation maps for "fractures," regions with rapidly changing orientation tuning. However, we did not find a consistent relationship between these fractures and the ocular dominance columns (12). For each orientation, we also attempted to image preferences for the direction of motion, but did not observe any differential response. These results imply that directionality is not organized in a columnar fashion.

We found that our ocular dominance maps also contained the information necessary to visualize the cytochrome oxidase blobs of

D. Y. Ts'o, R. D. Frostig, E. E. Lieke, The Laboratory of Neurobiology, The Rockefeller University, New York, NY 10021.

A. Grinvald, IBM, Research Division, Yorktown Heights, NY 10598; The Laboratory of Neurobiology, The Rockefeller University, New York, NY 10021; and the Weizmann Institute of Science, Israel.

V1. The blobs could be seen by producing a map of the regions of striate cortex that have highly monocular responses. Using a simple recoding of the ocular dominance map (Fig. 2, A and B), we derived a map of monocularly (Fig. 2C); black represents the most monocular regions and white represents the most binocular regions. A comparison with cytochrome oxidase histology (Fig. 2D) shows an excellent match between these dark regions and the cytochrome oxidase blobs. This finding is consistent with the high degree of monocularly in the response properties of blob cells (5) and their position in the middle of the ocular dominance columns. Our results also suggest that the blobs represent small centers of monocularly within the ocular dominance column, supporting the notion that blob cells receive direct thalamic input (5, 6).

A majority of cells in V2 are binocular, but there has been a question as to the organization of ocular dominance in V2 (9, 23). In our images of the portion of V2 bordering V1, we found an absence of ocular dominance structure (Fig. 1B). The uniform appearance of the map in V2 indicates the absence of large clusters or columns of cells with strong eye preference in V2. Thus the ocular dominance organiza-

tion in V2 is distinctly different from that of V1. 2-Deoxyglucose studies of ocular dominance in macaque have also failed to reveal any macroscopic organization of ocular dominance in V2 (24, 25). One electrophysiological study has suggested that occasionally individual units and clusters of units in V2 are dominated by input from one eye and that there are often rapid shifts in ocular dominance, even within the same vertical penetration (26).

It has been common practice to subtract the results from two opponent stimulus conditions (for example, left eye–right eye or vertical–horizontal orientation) to produce a map displaying the difference in response between the two stimulus conditions (12, 15). This strategy is excellent for imaging nonoverlapping regions that are selectively activated by the two stimulus conditions. However, the subtraction method may hide overlapping regions that are activated by both stimulus conditions. To circumvent this problem and more thoroughly analyze the patterns of activity due to a single stimulus condition, we compared the response to stimulation of one eye to the no stimulus condition (Fig. 1D). This approach revealed distinct patterns in V2 that were not seen in the original subtraction

analysis (Fig. 1B). The darkened bands in Fig. 1D interdigitate between left and right eye conditions in V1, as expected from the ocular dominance map in Fig. 1B. In V2, however, the darkened regions of the left and right eye maps overlap (25).

Comparison of these overlapping darkened regions in V2 with cytochrome oxidase histology (Fig. 3, A and B) showed that these regions of increased activity due to stimulation of either eye coincide with the thick and thin stripes of V2. This finding is reasonable because the presence of elevated concentrations of cytochrome oxidase probably indicates regions of long-term elevated activity. In spite of the distortions introduced by histological processing there was a close match between the optical imaging maps and the cytochrome oxidase histology of the stripes of V2. The two methods are quite different: the optical imaging technique integrates an optical signal of activity from a range of cortical depths spanning a fraction of a millimeter. In contrast, the histological data is obtained from a single 30- $\mu\text{m}$  section, showing the activity of a mitochondrial enzyme. As is true with cytochrome oxidase histology in macaque (9, 24), it was not always possible to tell which stripes were thick and which were thin with the use of this optical imaging strategy.

We were, however, able to distinguish between sets of stripes on the basis of functional properties, such as orientation tuning. The organization of orientation specificity in V2 appears to be different than that seen in V1 (Fig. 3C). The difference is best seen in this “polar” orientation map that includes the sharpness of the orientation tuning (magnitude) as well as the optimal angle. Regions of larger diameter modules (500- $\mu\text{m}$  versus 250- $\mu\text{m}$  diameter) with more uniform orientation tuning (as shown by a region of uniform color in the pseudocolor maps) are interspersed among regions with ill-defined orientation tuning (dark-coded regions). These larger modules are likely to correspond to the observation from electrophysiological studies, which found that recordings with tangential electrode penetrations in V2 often encountered long stretches (400 to 1000  $\mu\text{m}$ ) of cells with very similar orientation preferences, followed by abrupt shifts in orientation tuning (9). This orientation map, then, represents a two-dimensional view of the organization of orientation specificity hinted at in one dimension by tangential electrode penetrations.

The implications of the findings of large regions of uniform and strong orientation tuning in some regions of V2 is unclear, considering the presumptive need for a complete coverage and orientation sampling of the visual field. The larger iso-orientation

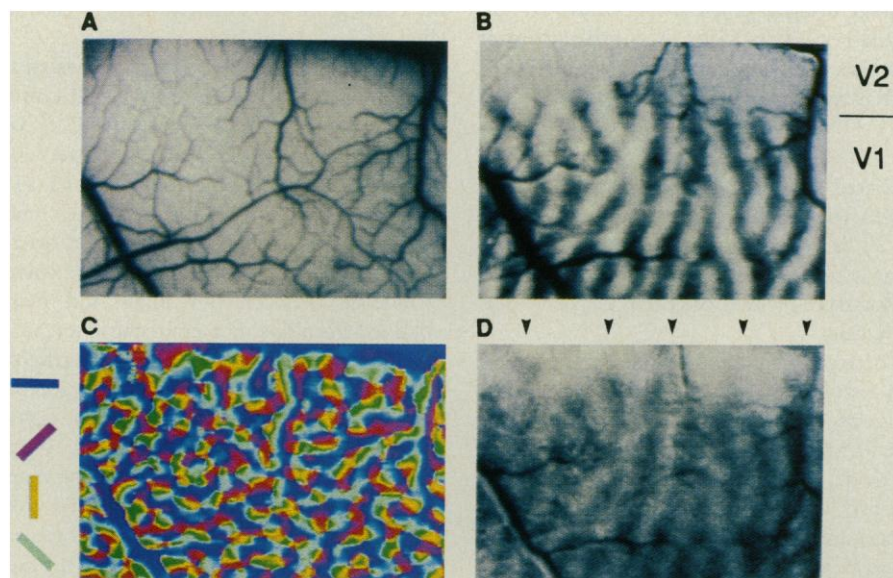
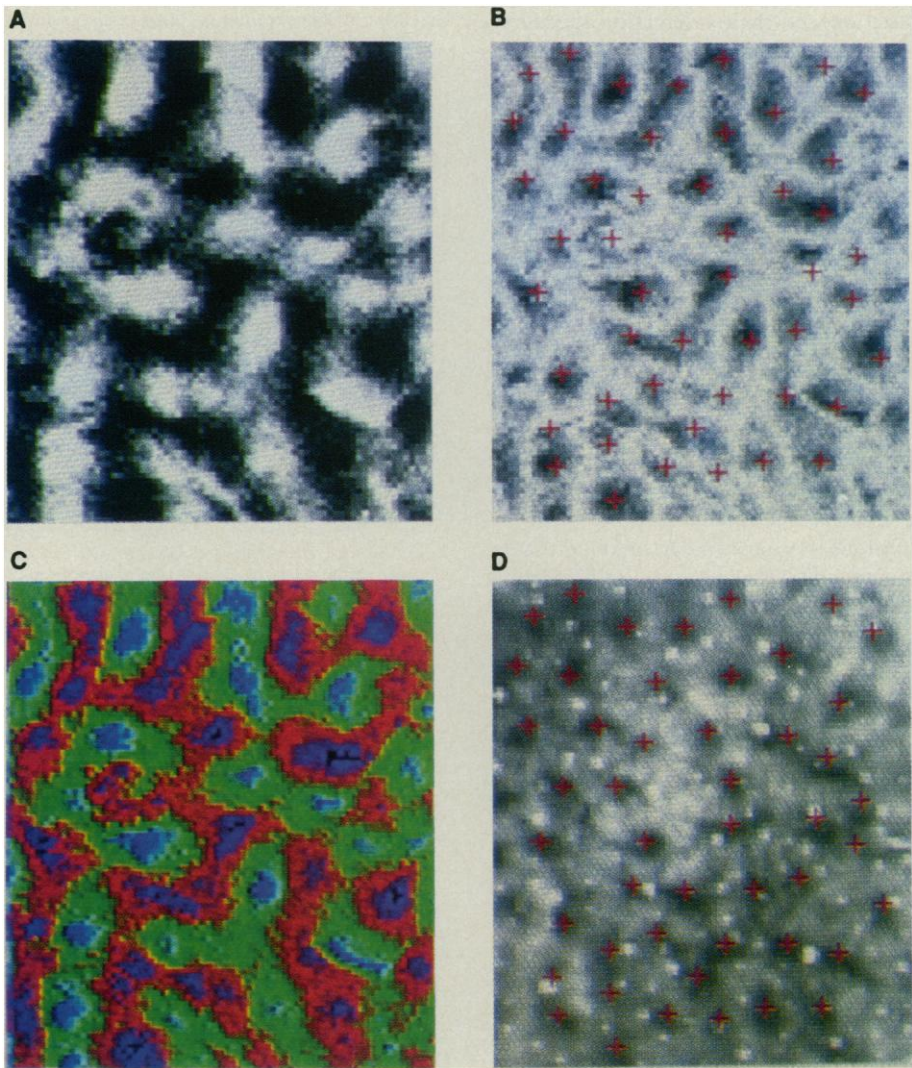


**Fig. 1.** (A) A CCD image of a 9 mm by 6 mm portion of macaque visual cortex, including a 1.5-mm strip of V2 up to the lunate sulcus (top edge), and V1, lying posterior to V2. We illuminated the cortex with green light (540 nm), for this image enhanced the contrast of the surface vasculature. (B) The optical recording map of ocular dominance from the same portion of visual cortex. The dark bands represent columns dominated by the left eye and the light bands, the right eye. There is an apparent absence of ocular dominance structure in the imaged strip of V2 (topmost 1.5 mm). The perpendicular arrangement of the ocular dominance columns relative to the V1/V2 border is also evident. (C) A map of orientation tuning produced by vector combination of frames acquired during stimulation with four orientations: 0°, 45°, 90°, and 135°. Only the preferred angle is displayed (coded in color, as shown). No information of sharpness of orientation tuning nor response strength is incorporated. (D) Image of activity (darkening) due to left eye stimulation as compared to the no stimulus condition (right eye map not shown). Without the subtraction procedure used for the ocular dominance map, patterns of increased activity can also be seen in V2. These bands (arrows) in V2 colocalize with the cytochrome oxidase-rich stripes.

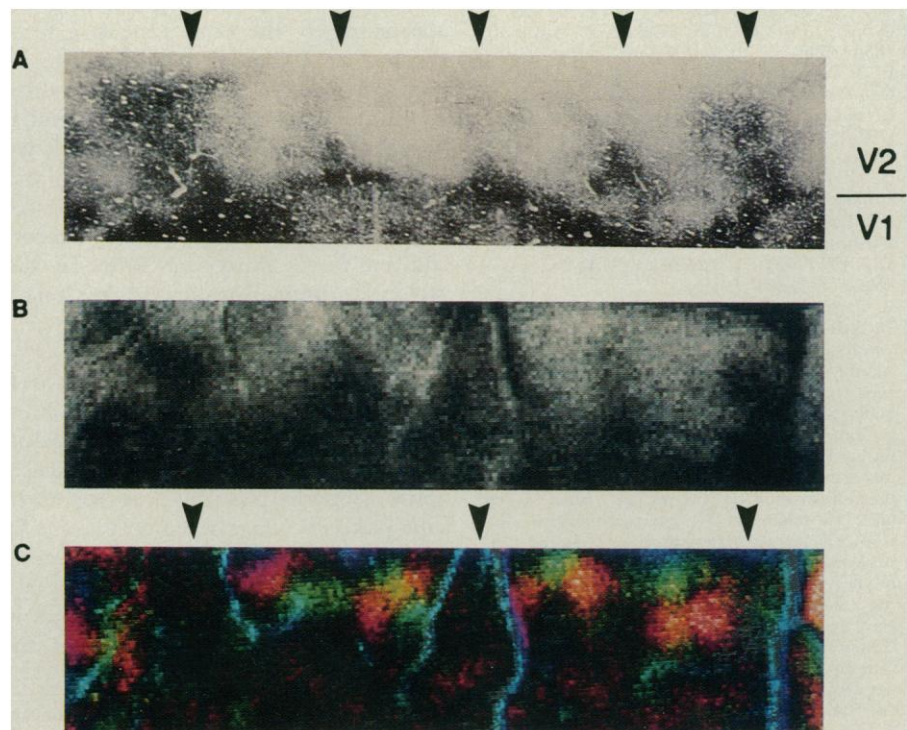
**Fig. 2.** The imaging of cytochrome oxidase-rich blobs by examining regions of highly monocular responses. (A) An ocular dominance map of V1 (3.5 mm by 4.5 mm field of view). This map was color-coded (B) such that left eye-dominated activity is red, right eye is green, and the extremes of left eye- or right eye-dominated activity are blue. These blue regions lie in the middle of both ocular dominance bands and correspond to centers of high monocular activity. (C) A recoding of the map in (B), producing a map of monocular activity, where the darker regions are monocular and the whiter regions are binocular. This map was then compared to the postmortem cytochrome oxidase histology (D). Cross marks were placed on the blobs seen in the histology (D). This pattern of crosses was then transferred to the map of monocular activity (C). Comparison of the monocular activity map with the cytochrome oxidase histology, showing excellent correspondence between the centers of monocular activity and the blobs.



modules in V2 (compared with V1) may be in part explained by the larger receptive fields and the larger scale of processing in V2. The functional significance of large orientation modules with uniform orientation tuning is not obvious, but is likely to be linked with another functional property, perhaps disparity tuning.

Between the large modules of uniform orientation tuning are regions with ill-defined orientation tuning. When compared with the image of the stripes of V2 from the same tissue (Fig. 3, B to D), it is apparent that these regions in V2 with ill-defined orientation tuning coincide with a subset of the stripes of V2 [probably the thin stripes, since they have been shown to contain unoriented cells (8, 9)]. Thus, by combining the imaging strategy described above for imaging the V2 stripes with an examination of the orientation map in V2, we have been able to distinguish between the thick and thin stripes in the living brain, and support the findings of other investigators (8, 9) that the stripes of V2 differ in their functional spe-

**Fig. 3.** Confirmation of the optical imaging of the V2 stripes with the corresponding cytochrome oxidase histology and the relation between orientation tuning and the stripes of V2. (A) The cytochrome oxidase histology showing a match of the bands of increased activity seen in the optical map with the stripes (arrows). (B) Optical imaging map showing five of the V2 stripes (the top portion of the same image as Fig. 2B, the lunate sulcus is at the top edge). (C) Orientation tuning in V2. A difference in the organization of orientation tuning between V1 and V2 becomes apparent when the orientation map is recoded such that the color of a pixel indicates the preferred orientation while the intensity indicates the sharpness of the tuning (a polar map, color coded as in Fig. 1C). There are prominent regions of uniform orientation tuning in V2; in addition there are other V2 regions (arrows) with poor orientation tuning that coincide with the locations of every other stripe, beginning with the stripe on the far left.



cialization and their orientation specificity.

An accumulation of anatomical, physiological, and psychophysical data suggests that the visual processing of form, color, depth, and motion is segregated into separate pathways and structures in the visual cortex (27). We have shown that high spatial resolution optical imaging can be used to visualize many of these components of visual processing in vivo, using activity-dependent intrinsic signals. We have also shown that these subdivisions of visual processing (for example, the blobs of V1 and the thick and thin stripes of V2) can be distinguished by their specialized functional properties and can now more easily be studied by the use of optical maps for guiding single-unit recording and tracer injections (26).

*Note added in proof:* We have found that by imaging with a shallow depth of field below the cortical surface, blood vessel artifacts can be nearly eliminated (28).

#### REFERENCES AND NOTES

1. V. S. Mountcastle, *J. Neurophysiol.* **20**, 408 (1957).
2. D. H. Hubel and T. N. Wiesel, *J. Physiol.* **160**, 106 (1962).
3. M. T. T. Wong-Riley, *Brain Res.* **171**, 11 (1979).
4. J. C. Horton and D. H. Hubel, *Nature* **292**, 762 (1981). J. C. Horton, *Philos. Trans. R. Soc. London* **304**, 199 (1984).
5. M. S. Livingstone and D. H. Hubel, *J. Neurosci.* **4**, 309 (1984).
6. ———, *Proc. Natl. Acad. Sci. U.S.A.* **79**, 6098 (1982).
7. R. B. H. Tootell et al., *Science* **220**, 737 (1983).
8. E. A. De Yoe and D. C. Van Essen, *Nature* **317**, 58 (1985).
9. D. H. Hubel and M. S. Livingstone, *J. Neurosci.* **7**, 3378 (1987).
10. A. Grinvald, L. Anglister, J. A. Freeman, R. Hildesheim, A. Manker, *Nature* **308**, 848 (1984). H. S. Orbach, L. B. Cohen, A. Grinvald, *J. Neurosci.* **5**, 1886 (1985).
11. P. De Weer and B. M. Salzberg, *Optical Methods in Cell Physiology* (Wiley, New York, 1986). L. B. Cohen and S. Leshner, *Soc. Gen. Physiol. Ser.* **40**, 71 (1986). A. Grinvald, R. D. Frostig, E. E. Lieke, R. Hildesheim, *Phys. Rev.* **68**, 1285 (1988).
12. G. G. Blasdel and G. Salama, *Nature* **321**, 579 (1986).
13. J. S. Kauer, *ibid.* **331**, 166 (1988).
14. B. Chance, P. Cohen, F. Jobsis, B. Schoener, *Science* **137**, 499 (1962). D. K. Hill and R. D. Keynes, *J. Physiol.* **111**, 304 (1949).
15. A. Grinvald et al., *Nature* **324**, 361 (1986).
16. D. Y. Ts'o, R. D. Frostig, E. E. Lieke, A. Grinvald, *Abst. Soc. Neurosci.* **14**, 898 (1988).
17. Monkeys (*Macaca fascicularis*) were initially anesthetized with ketamine HCl (20 mg per kilogram of body weight, intramuscular) followed by sodium pentothal (20 mg/kg, intravenous supplemented by further injections as needed). The animal was then cannulated through a tracheotomy, paralyzed with vecuronium bromide (0.1 mg kg<sup>-1</sup> hour<sup>-1</sup>), and artificially respired. The electrocardiogram, electroencephalogram, temperature, and expired CO<sub>2</sub> were monitored throughout the entire experiment.
18. A hole was made in the skull above the striate cortex and a stainless steel optical chamber was cemented over the hole. After the dura was opened, the chamber was sealed with a glass cover plate and filled with silicone oil. Single-unit electrical recordings were made through a rubber gasket in the glass cover plate.
19. A slow-scan CCD camera (Photometrics, Ltd.) was

mounted above the optical chamber and provided digitized images with a signal-to-noise ratio of better than 1400:1 and a spatial resolution of 192 by 144 pixels. The surface of the cortex was illuminated with a 630-nm light (20). Five to 10 frames were acquired within 3 s, during a visual stimulus presentation, followed by a 10-s intertrial interval.

20. R. D. Frostig, E. E. Lieke, D. Y. Ts'o, A. Grinvald, *Proc. Natl. Acad. Sci. U.S.A.*, in press.
21. Data analysis began with the summation of frames acquired for each type of visual stimulus. We then divided each of these summed images by the sum of the blank stimulus trials, to minimize the effects of uneven illumination and other common mode features. The resultant summed, blank-adjusted images were subtracted from each other as appropriate for the particular functional property under study (for example, for ocular dominance, the summed, blank-adjusted images from the left eye were subtracted from the right-eye images). The color map of the display was set for either linear 8-bit gray scale translation, or sometimes, pseudo-color mapping designed to facilitate interpretation.
22. In a typical experiment, adequate orientation maps were obtained after cortical images were averaged for 30 min. The signal-to-noise ratio (S/N) of our maps seems at least as good as similar maps from 2-DG studies. For example, a comparison between the densitometry analysis of a 2-DG map of orientation tuning and the optical imaging map of orientation showed that the 2-DG map had a S/N of roughly 5 and the optical imaging map had a S/N of roughly 7 (for 45 min of data acquisition). We estimate that the spatial resolution of this imaging technique is 100 to 150 μm. The functional maps obtained with optical imaging are very reproducible. For example, a pixel-by-pixel comparison between two separate

orientation maps obtained in interlaced fashion showed that 85% of the pixels reported orientations within 20° of each other, and 95% within 30°. Similar results were obtained in comparisons between pairs of orientation maps collected several hours apart, and between pairs of maps of other functional properties. Our optical imaging maps have been confirmed with extensive single-unit recordings (15, 18).

23. D. H. Hubel and T. N. Wiesel, *Nature* **225**, 41 (1970). G. F. Poggio and B. Fischer, *J. Neurophysiol.* **40**, 1392 (1977). J. S. Baizer, D. L. Robinson, B. M. Dow, *ibid.*, p. 1024.
24. R. B. H. Tootell and S. L. Hamilton, *J. Neurosci.* **9**, 2620 (1989).
25. H. R. Friedman, C. J. Bruce, P. S. Goldman-Rakic, *ibid.*, p. 4111.
26. D. Y. Ts'o, C. D. Gilbert, R. D. Frostig, A. Grinvald, T. N. Wiesel, *Abst. Soc. Neurosci.* **15**, 161 (1989); D. Y. Ts'o, C. D. Gilbert, T. N. Wiesel, *ibid.*, in press.
27. S. M. Zeki, *Nature* **274**, 423 (1978). S. Shipp and S. Zeki, *ibid.* **315**, 322 (1985). M. S. Livingstone and D. H. Hubel, *J. Neurosci.* **7**, 3416 (1987). D. C. Van Essen and J. H. R. Maunsell, *Trends Neurosci.* **6**, 370 (1983).
28. D. Maloney, D. Shoham, E. Ratzlaff, A. Grinvald, *Abst. Soc. Neurosci.*, in press.
29. We thank T. Wiesel, C. Gilbert, L. Katz, and S. Szapeli for their comments on the manuscript, K. Christian and G. Ratzlaff for technical support, P. Peirce for photography, and M. Carter and P. Joyce for histology. The work was supported by IBM Research Division, The Whitaker Foundation, and NIH grants EY05253, EY08240, and NS14716.

2 October 1989; accepted 10 May 1990

## Long-Term Synaptic Changes Produced by a Cellular Analog of Classical Conditioning in *Aplysia*

DEAN V. BUONOMANO AND JOHN H. BYRNE

A change in synaptic strength arising from the activation of two neuronal pathways at approximately the same time is a form of associative plasticity and may underlie classical or Pavlovian conditioning. A cellular analog of a classical conditioning protocol produces short-term associative plasticity at the connections between sensory and motor neurons in *Aplysia*. A similar training protocol produced long-term (24-hour) enhancement of excitatory postsynaptic potentials (EPSPs). EPSPs produced by sensory neurons in which activity was paired with a reinforcing stimulus were significantly larger than unpaired controls 24 hours after training. Thus, associative plasticity at the sensory to motor neuron connection can occur in a long-term form in addition to the short-term form. In this system, it should be possible to analyze the molecular mechanisms underlying long-term associative plasticity and classical conditioning.

CHANGES IN SYNAPTIC STRENGTH are believed to be the basis for short- and long-term memory. A particularly important form of synaptic modification is associative plasticity. Associative synaptic plasticity occurs when activation of a neuron or of a neural pathway at approximately the same time as the activation of a second neural pathway induces changes in synaptic efficacy not observed when the

same pathways are activated noncontiguously. Neuronal changes resulting from associative plasticity are of particular interest, because they are likely to underlie classical or Pavlovian conditioning (1) and because theoretical work indicates that associative plasticity may function as a fundamental "learning rule" for more complex phenomena such as higher order forms of classical conditioning, associative memories, and self-organization of neural networks (2). Although various instances of short-term (minutes to hours) associative synaptic plasticity have

Department of Neurobiology and Anatomy, University of Texas Medical School, Houston, TX 77225.